Thermo-responsive nanofibrous composite membranes for efficient self-cleaning of protein foulants

Thermo-responsive Nanofibrous Composite Membranes for Efficient Self-Cleaning of Protein Foulants

Anbharasi Vanangamudi[1,2], Ludovic F. Dumée[2], Elise Des Ligneris[2], Mikel Duke[1] and Xing Yang[1*]*

[1]Institute for Sustainable Industries & Liveable Cities, College of Engineering and Science, Victoria University, Melbourne, Australia

[2]Deakin University, Geelong, Institute for Frontier Materials, 75 Pigdons road, Waurn Ponds, 3216, Victoria, Australia

Corresponding Authors

*Ms. Anbharasi Vanangamudi

Email: anbharasi.vanangamudi@live.vu.edu.au; Tel.: +61 399 197 640

*Dr. Xing Yang

Email: xing.yang@vu.edu.au; Tel.: +61 399 197 690

Abstract

This study developed a self-clean thermo-responsive nanofibrous poly(vinylidene fluoride) (PVDF)/nylon-6,6/poly(N-isopropylacrylamide) (PNIPAAm) composite ultrafiltration membrane consisting of a nylon-6,6/PNIPAAm functional nanofibre layer integrated into a PVDF substrate. The morphological analysis showed the presence of electrospun nano-nets branching out from the main nanofibres as PNIPAAm concentration increased, affecting the pore size distribution and solute rejection. The PVDF/nylon-6,6/PNIPAAm membranes showed improved surface hydrophilicity below the low critical solution temperature (LCST) and strong thermo-switchability. With bovine serum albumin (BSA) as the model foulant, the rejection of the 4 wt% PNIPAAm membranes was greatly improved to above 96%. Through a two-cycle ultrafiltration study using feed solution containing BSA and $CaCl_2$, the membrane with 4 wt% PNIPAAm showed superior recovery of water permeance up to 97% assisted with temperature-change cleaning, compared to the control membrane that only recovered 56%. Filtration experiments with and without intermediate temperature-change cleaning proved that the anti-fouling mechanism of the PNIPAAm membranes was strongly associated with surface wettability and rapid conformation of PNIPAAm polymer chains induced by volume-phase transition, resulting in reduced protein adsorption and 'shaking-off' of the absorbed proteins from the membrane surface. Such smart responsive membranes have great potential for the development of easy-to-clean membranes for food and wastewater treatment.

Keywords: thermo-responsive; volume-phase transition; protein fouling; self-cleaning; ultrafiltration

1. Introduction

Continuous surface-contaminant interactions at the membrane interface during ultrafiltration (UF) causes accumulation of various contaminants instigated by membrane fouling arising from the interaction between membrane and solutes such as proteins, microbes, colloidal particles [1]. Fouling causes pore blockage and forms cake layer leading to rapid decline in membrane permeability, increase in cleaning frequency and eventually diminish membrane performance [2, 3]. Fouled membranes can be cleaned at regular intervals using chemicals such as acids and bases or backwashing [4]. Such cleaning disturbs the filtration process and the use of strong chemicals causes irreversible damage to the membrane, reducing membrane life time [5]. One of the most versatile approaches to mitigate fouling and self-clean the membranes is to alter the membrane surface chemistry by incorporating functional materials materials such as hydrophilic copolymers [6], biomolecules [7], amphiphilic copolymers [8], responsive materials [9], zwitterionic compounds [10] and metal oxides [11-13]. The anti-fouling mechanism is to utilize either the enhanced surface hydrophilicity or dynamic material property to repel hydrophobic foulants away from the membrane surface to reduce irreversible fouling [14, 15].

Thermo-responsive materials have been widely used to create smart surfaces for reversibly dynamic adsorption and desorption in drug delivery, solute separation and many other fields [9, 16-18]. Poly(N-isopropylacrylamide) (PNIPAAm) is a well-known temperature-sensitive polymer with a lower critical solution temperature (LCST) of about 32°C in an aqueous solution [19, 20]. Below the LCST, the PNIPAAm polymer chains are more hydrophilic and have an extended conformation in water. Above the LCST, the polymer chains become hydrophobic due to cleavage of hydrogen bonds between the amide groups of PNIPAAm and bound water, which is known as the volume-phase conformational transition (VPT) [21, 22]. Other than varying the surface wettability, the VPT is also known to induce a reversible rapid

stretching-shrinking effect of the polymer chains, driving the absorbed solutes to detach from the surface. Studies found that hydrophobic proteins tend to absorb onto PNIPAAm modified surfaces above the LCST and desorb below it [23, 24]. Partial or complete desorption of the absorbed proteins was observed using temperature or rinse cycling (i.e., temperature-change rinsing) due to the VPT mechanism. Hydrophilicity and segment mobility of polymer chain are known to be important factors for reducing protein adsorption [25]. The adsorption-desorption behaviour of proteins is determined by the surface wettability, functional groups and nano-topography [26, 27]. For example, a single-molecule kinetics of protein adsorption was proposed to explain the different adsorption behaviour of protein onto PNIPAAm grafted dense and porous nylon 66 films [28]. The results found that the protein attachment was less favourable on porous surface due to lower Gibbs free energy induced by increased surface roughness. Such findings have wider implications for developing self-cleaning membranes for liquid filtration.

In recent decade the concept of PNIPAAm smart interfaces has been extended to separation membranes for anti-fouling and easy cleaning purposes [29-31]. However, the understanding is still limited on the protein-membrane attachment behaviour under filtration conditions where cross-membrane penetration (mass transfer) occurs. Thus far only a handful of studies were reported on PNIPAAm based membranes with pore size in the UF range, where protein fouling is a significant issue. For example, PNIPAAm grafted polydopamine/polyethylene terephthalate (PET) UF membranes demonstrated reduced protein fouling with 90% flux recovery at 20°C compared to unmodified PET membrane showing only 76% flux recovery in the same cleaning conditions, attributed to the improved surface hydrophilicity [32]. However, the temperature switchability of the membrane was not investigated. In another study, the PNIPAAm grafted PVDF/TiO_2-g-PNIPAAm nanocomposite membrane showed increased flux of 212 $L.m^{-2}.h^{-1}$ at 40°C from a flux of 108

94 $L.m^{-2}.h^{-1}$ at 23°C due to hydrophilic/hydrophobic transition of PNIPAAm polymer brushes
95 resulting in "open" state of pores above LCST (40°C) [33], demonstrating a flux recovery of
96 92% compared to 47% for the control PVDF membranes. The PNIPAAm grafted polyethylene
97 (PE) membrane was developed together with a simple temperature-change (25°C/35°C)
98 cleaning method to utilize the reversible VPT mechanism demonstrating 97% flux recovery
99 after fouled by model protein BSA [34]. Similarly cleaning strategy was used for the
100 PNIPAAm-grafted ZrO_2 membrane that showed 80% flux recovery [31]. Overall, in the above
101 studies, the self-cleaning behaviour of the membrane was attributed to the enhanced
102 hydrophilicity below LCST via the addition of PNIPAAm, facilitating foulants desorption.
103 While few other studies hypothesized that the rapid stretching-shrinking effect during the VPT
104 of PNIPAAm polymer chains is responsible for loosening and shaking off protein foulants.
105 Also the above-mentioned PNIPAAm based membranes are prepared by graft polymerization
106 method that is complex and requires highly-specialized treatment. Facile fabrication methods
107 and versatile substrates with abundant moieties for high density functionalization are still
108 needed for developing dynamic PNIPAAm-based membranes for effective fouling control.

109 In this study, a facile electro-spinning method is used to fabricate thermo-responsive
110 PVDF/nylon-6,6/PNIPAAm composite membrane to create desirable nanofibrous topography
111 and pore structure for UF applications. The electrospun nanofibrous layer with nylon/
112 PNIPAAm blend is expected to exhibit enhanced hydrophilicity and thermal responsivity, as
113 result of the high density of surface functional moieties due to its high surface to volume ratio.
114 The impact of the PNIPAAm concentration on the nanofibre structure, thermo-responsive
115 properties and membrane performance will be studied. Specifically, the thermo-switchability
116 of the PNIPAAm containing membranes will be evaluated via contact angle measurements.
117 The anti-fouling and self-cleaning mechanisms of the membranes will be revealed through a

series of filtration experiments with model foulant BSA, assisted with intermediate temperature-change cleaning with clean water.

2. Experimental

2.1. Materials and Chemicals

PVDF Kynar 761 grade (melting point 165-172°C) was purchased from Arkema Pte. Ltd., Singapore. The following chemicals were purchased from Sigma Aldrich and used as-received: poly (N-isopropylacrylamide) (PNIPAAm) (M_w 113 g/mol, M_n 40,000), polyamide-6,6 (nylon-6,6) (M_w 262.35 g/mol), poly(vinylpyrrolidone) (PVP-K-40) (M_w 40,000), bovine serum albumin (BSA) (M_w 66 kDa) as model protein, formic acid (>95%), N,N'-dimethylacetamide (DMAC) (99.8%), 75% ethanol, glycerol (>99.5%), calcium chloride ($CaCl_2$) and sodium chloride (NaCl). Deionized (DI) water was obtained from the Milli-Q plus system (Millipore, Bedford, MA, USA).

2.2. Fabrication of thermo-responsive PVDF/nylon-6,6/PNIPAAm composite membrane

The thermo-responsive PVDF/nylon-6,6/PNIPAAm composite membranes were prepared based on the fabrication procedure similar to our previous work, where the PVDF cast layer was used as the substrate to achieved desirable pore structure in UF range, as well as to strengthen the mechanical property and avoid deformation issue of free-standing nanofire membranes [13]. Briefly, the membranes were prepared by three successive steps, (1) electrospinning of blend solution of 10 wt% nylon-6,6 and different PNIPAAm concentrations (1 to 7 wt% PNIPAAm dispersed in nylon-6,6 solution), carried out at fixed spinning conditions a voltage of 17 kV and flow rate of 0.25 mL/h with 150 mm tip to collector distance to obtain thermo-responsive functional nanofibre mat, (2) conventional casting of the PVDF

dope solution with previously optimized composition of 18 wt% PVDF and 8 wt% PVP in DMAC solvent to ensure consistent pore structure of the substrate layer [13], which was prepared by continuous stirring at 50°C overnight, on to the nanofibre mat and (3) phase inversion of the composite film prepared from step (1) and (2) by immersing into a coagulation tank of DI water at 25°C to remove residual solvent. The nascent membranes were post-treated by immersing in to a mixture of glycerol, ethanol and DI water in the ratio 2:1:2 (vol%) and was then dried finally before characterisation. Similarly, the control PVDF/nylon-6,6 membrane was prepared without the addition of PNIPAAm.

2.3. Membranes characterisation

It is noted that the PVDF substrate was made of the same dope composition (Section 2.2) for all membranes, which was previously optimized to ensure consistent pore structure [13], thus the characterization of the current composite membrane was mainly focused on the functional layer of nylon-6,6/chitosan nanofibres.

The surface morphology of the as-prepared PVDF/nylon-6,6/PNIPAAm membranes was observed using scanning electron microscopy (SEM) (ZEISS SUPRA 55VP, Germany) with an accelerating voltage of 5 kV and working distance of 10 mm. Prior to imaging using SEM, the membrane samples were sputter coated with 5 nm gold layer in high vacuum using a Leica EM ACE600. The average nanofibre diameters of the membranes and density of nano-nets were evaluated from the SEM images using ImageJ software. Transmission electron microscopy (TEM) imaging was conducted using JEOL TEM 2100F, operating at an accelerating voltage of 200 kV and beam current of 130 µA to study the distribution of PNIPAAm (lighter regions with M_w: 113 g/mol) and nylon-6,6 (darker regions with M_w: 262 g/mol) in the nanofibre mat. The TEM samples were mounted on 300 nm mesh copper grids coated with carbon formvar.

The dynamic water contact angles (CA_w) of the as-prepared membranes were measured using an optical contact angle meter CAM101 (KSV Instruments, Finland) to examine the switchable surface hydrophilicity at 22°C (below LCST) and 50°C (above LCST). The required temperature of the membrane samples was achieved by adjusting the voltage of the source meter connected to the heating pad on which the samples are mounted. Prior optimisation of corresponding temperatures and feed voltages of the heating mats were established before mounting the heating pad on the contact angle meter. Each membrane sample was cut into thin rectangular strips, and the two edges of the membrane were pasted onto the heating pad with sticky tape. A glass syringe filled with DI water was then used to dispense about 4 µL droplet through a needle onto the membrane surface. Each measurement was recorded every 5 s over the duration of 60 s.

The mean pore size and pore size distribution of the membranes were measured using a Porometer 3Gzh from Quantachrome. The membrane samples of 25 mm diameter each were completely wetted in the Porofil^{TM} liquid before analysis and then placed in the sample holder. Each sample was subjected to pressures from 6.4 to 34 bar for wet and dry run to measure the mean pore size. The pore size was measured three times for each membrane to obtain the average pore size. The mechanical properties of the membranes were studied using an Instron universal materials testing machine (Model 3360) with a load cell of 50 N and a loading velocity of 25 mm/min. Each membrane sample of dimension of 10 x 60 mm^2 was tested three times to achieve average values of tensile stress and strain.

2.4. Membrane performance and fouling studies

The clean water permeance was determined using a dead-end filtration cell with an effective membrane area of 8.55 x 10^{-4} m^2 at room temperature (22°C). The membrane was placed in dead-end stirred cell and 50 mg/L NaCl feed solution was allowed to flow through the

membrane at 100 kPa pressure created using compressed nitrogen. The amount of permeate collected per minute was recorded at room temperature and the clean water permeance (P) in $L.m^{-2}.h^{-1}.bar^{-1}$ was calculated. The measurement was repeated three times and averaged to provide a mean permeance value. Similarly, feed solution containing 1000 mg/L BSA and 50 mg/L NaCl in DI water was filtered through the membrane to measure the flux as well as rejection 'R' of BSA in percentage (%) [13].

The fouling resistance and self-cleaning ability of the thermo-responsive membranes was evaluated using a cross flow UF set up having an effective membrane area of 42 x 10^{-4} m^2 and flow velocity of 12.6 $cm.s^{-1}$. BSA has a molecular weight of 66 kDa and is used as a model protein foulant in filtration studies [35]. Here, the prepared feed solution contained 1 mg/mL BSA, 7 mM NaCl and 1 mM $CaCl_2$ in DI water. The $CaCl_2$ added to the feed solution represents the practical fouling environment through forming Ca^{2+}-protein complexes [36]. The membranes were initially exposed to 15 min of compaction using DI water at 120 kPa at RT. Each UF experiment had 2 cycles and each cycle included the filtration of the prepared feed solution at 22°C for 1 h followed by an intermediate temperature cleaning with DI water at 50°C for 15 min. To confirm the thermo-responsive effect of the membrane, two-cycle fouling experiments at a constant solution temperature of 22°C without cleaning were performed and compared with the same experimental condition including with intermediate temperature cleaning at 22°C.

To measure protein fouling, the rate of permeance decline (R_{PD}) after each cycle was calculated using the equation,

$$RPD\ (\%) = \left[1 - \left(\frac{P_{e(n)}}{P}\right)\right] * 100 \qquad (1)$$

where $P_{e(n)}$ is the final feed permeance in n^{th} cycle. Further, to study the self-cleaning property of membranes, the permeance recovery after the intermediate temperature cleaning at 50°C was calculated using the equation,

$$PRR\ (\%) = \frac{P_{w(n)}}{P} * 100 \quad (2)$$

where $P_{w(n)}$ is the clean water permeance in n^{th} cycle. Finally, the surfaces of thermo-responsive and control membranes after 2 cycles of filtration were imaged using SEM to visualise and compare the antifouling and self-cleaning properties.

3. Results and discussion

3.1. Membrane pore and nanofibre morphology and correlation to mechanical properties

With the PNIPAAm concentrations varied in the dope solution of nylon-PNIPAAm mixture, the surface morphology of a series of thermo-responsive membranes was examined using SEM images as shown in Figure 1. Figure 1a presents the surface of the control membrane without PNIPAAm; while Figure 1b to 2h indicate surfaces of membranes containing 1 to 7 wt% PNIPAAm. The SEM images illustrate that the size of the nanofibres increases and the uniformity of the fibre size varies with increasing PNIPAAm dosage at fixed electro-spinning spinning conditions (Section 2.2), mainly due to the change in dope composition and viscosity. Membranes with no PNIPAAm and 1 wt% PNIPAAm show homogenous nanofibres with diameters of 83 ± 27 nm and 93 ± 18 nm, respectively; whereas, membranes containing 2 to 7 wt% PNIPAAm show non-homogenous fibre diameters and the presence of nano-branched structure called nano-nets, which was branched out from the larger nanofibres. The main larger fibre diameters for membranes with 2 to 7 wt% PNIPAAm were measured and are given in Table S1. It was found that the deviations of the main fibre diameters are quite large at high

PNIPAAm concentration such as 6 wt% (812 ± 409 nm) and 7 wt% (500 ± 216 nm). The non-uniformity of the fibre diameter is possibly related to the higher degree of non-homogeneity of the nylon-6,6/PNIPAAm solution, due to the agglomeration of PNIPAAm at high concentration [37]. Such finding is consistent with the current experimental observation on the increased cloudiness of the nylon-6,6/PNIPAAm solution at increased PNIPAAm concentration. It was observed that the development of branched nanofibres (i.e., nano-nets) increased significantly with increasing PNIPAAm concentration, i.e., 1 wt% PNIPAAm was not sufficient to create nano-nets; while 2-7 wt% PNIPAAm was effective in creating the nano-net structure. The formation of nano-nets can be attributed to the reduced intermolecular force between the nylon-6,6 molecules and increased viscosity with the addition of PNIPAAm polymer, causing the splitting of the jet during electrospinning [37, 38]. Overall, the integration of the PVDF substrate and nylon/PNIPAAm nanofibre layer was considered similar to that previously reported electro-spun composite membranes, where the cross-section images indicated a optimal degree of penetration of nanofibre layer into the substrate and hence improved layer compatibility and stability at selected dope compositions [13].

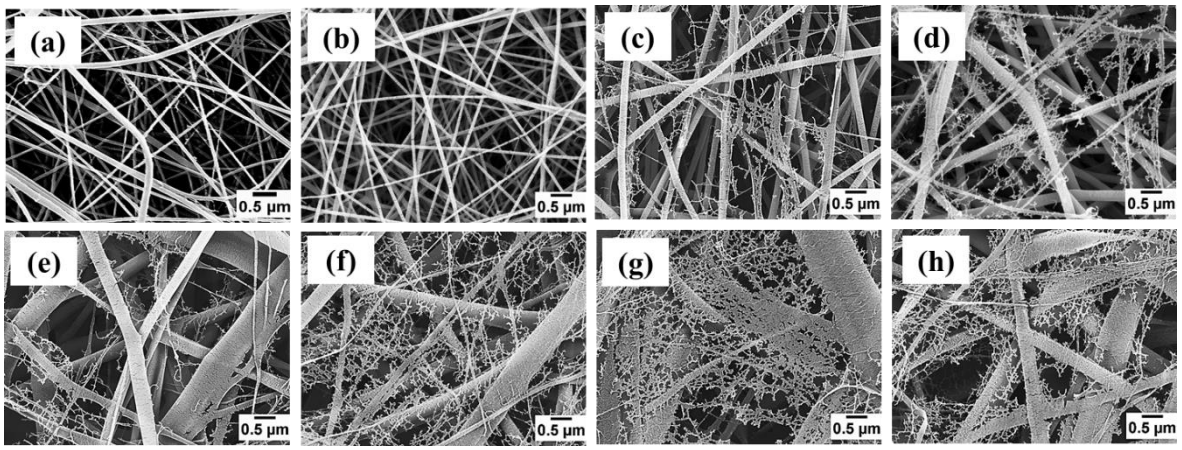

Figure 1. SEM images of PVDF/nylon-6,6/PNIPAAm membrane surfaces with PNIPAAm of various concentrations (a) no PNIPAAm, (b) 1 wt%, (c) 2 wt%, (d) 3 wt%, (e) 4 wt%, (f) 5 wt%, (g) 6 wt% and (h) 7 wt%.

However, the distribution of nano-nets on the membrane surface was found to be non-homogenous. As shown in Figure S1, the surface density coverage of the nano-nets for membranes prepared with 2 to 7 wt% PNIPAAm was found to be <10%, that may affect the water flux and rejection performance of the membranes. The distribution of PNIPAAm in the nanofibres was studied by performing TEM analysis on the fibres as given in Figure S2. It was noticed that the PNIPAAm appeared to be distributed homogenously across the nanofibre and no phase separation between the nylon-6,6 and PNIPAAm polymers was visible at any of the concentrations. Further, the average thickness of the as-prepared membranes was presented in Table S1 and found to increase from 247 ± 7 to 272 ± 12 µm for membranes with increasing PNIPAAm concentration from 1 to 7 wt%, respectively.

As the composite membrane consisted of a PVDF substrate and a nylon/PNIPAAm functional layer, the pore structure formed by the nanofibres on the surface (Figure 1) does not fully represent the pore structure of the entire membrane. Thus, the mean pore sizes and overall pore size distributions of the composite membranes were measured separately using a capillary-flow porometer [13]. Figure 2 compares the differential pore distributions of the as-prepared membranes in terms of pore diameters that impacts the membrane permeability and selectivity. The membranes containing no PNIPAAm and 1 wt% PNIPAAm exhibit similar narrow distribution curves; while the other membranes containing 2 to 7 wt% PNIPAAm have wider bimodal distribution curves indicating the co-existence of small and large pores, which are possibly contributed by the respective main nanofibres and the nano-nets, as observed in Figure 1c-1h. The results show that these pores can be altered by varying the PNIPAAm concentration of the nanofibre layer, where for all as-prepared membranes the PVDF substrate remained at its optimal structure developed previously [13]. The mean pore size distributions of the membranes are given in Table S1. It can be observed that the membranes with no PNIPAAm and 1 wt% PNIPAAm content showed almost similar mean pore size of about 47 nm due to

279 the similar nanofibre arrangement as noticed from SEM images in Figure 1a-1b. Further, the
280 mean pore sizes of the membranes with 2 to 4 wt% PNIPAAm decreased with increasing
281 PNIPAAm concentration due to the formation of nano-nets that contributed to smaller pores
282 (as seen from Figure 1c-1e). However, the mean pore sizes for membranes with 5 to 7 wt%
283 PNIPAAm increased instead, possibly due to the larger nanofibre diameter (as observed from
284 Figure 1f-1h) that produced larger pores. Hence, the non-homogenous distribution of nano-nets
285 on the membrane surface contributed to bimodal pore size distribution and the overall pore size
286 of the membrane was influenced by the combined structure of large main nanofibres, branched
287 nano-nets and the PVDF substrate.

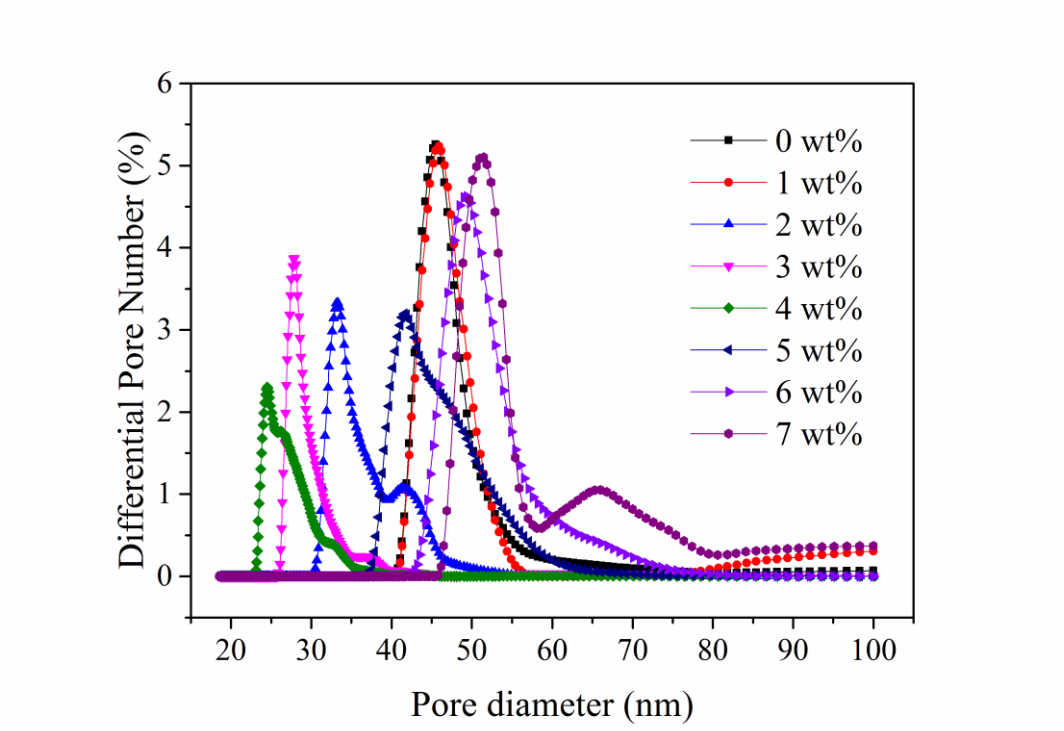

288

289 **Figure 2.** Differential pore number (in %) distributions of PVDF/nylon-6,6/PNIPAAm
290 membranes containing 1 to 7 wt% PNIPAAm and PVDF/nylon-6,6 membrane without
291 PNIPAAm.

292

293 The mechanical properties of the membranes indicate material strength and elasticity that are
294 essential for widespread applications. The as-prepared membranes were evaluated for tensile

stress as a function of strain at break (%) as presented in Figure S3. The mechanical properties are strongly dependent on the morphological structure of composite membranes and the interaction among the nanofibres. Figure S3 demonstrates that the tensile strength of the PVDF/nylon-6,6/PNIPAAm membranes with PNIPAAm concentration from 1 to 6 wt% was higher than the control membrane possibly due to the main fibres acting as skeleton and the nano-nets acting as connectors bonded with the main fibres through entanglement [39]. Increased stress and strain noticed for the membrane with 4 wt% PNIPAAm compared to other as-prepared membranes was attributed to better interconnectivity (bonding) between the main nanofibres and the nano-nets in the membrane. However, the highest modulus of elasticity observed for membrane with 6 and 7 wt% PNIPAAm (Table S1) represents greater stiffness of the membrane compared to other membranes, due to higher PNIPAAm concentration that can agglomerate and form interconnected bonding between the nanofibres and nano-nets.

3.2. Impact of PNIPAAm loading on membrane wettability and thermo-switchability

The dynamic contact angles of water (CA_w) were measured over 60 s at 22°C and 50°C and are given in Figure 3a and 3b, respectively, to evaluate the surface wettability of the thermo-responsive PVDF/nylon-6,6/PNIPAAm membranes. The CA_w for the PNIPAAm containing membranes at 22°C exhibit a faster attenuation compared to the control membrane, as shown in Figure 3a. This fast decreasing tendency was due to the addition of PNIPAAm that have a hydrophilic extended conformation below its LCST (32°C) which absorbs water drop by forming hydrogen bond between the amide groups of PNIPAAm and water. Also, it was noticed that at 22°C, the membranes with 3 and 4 wt% PNIPAAm reached the lowest CA_w, 11.6° and 10.5° respectively, after 60 s, indicating improved hydrophilicity. While the membranes with no PNIPAAm presented the highest final CA_w of 42.4°. This was attributed to the sufficient addition of PNIPAAm in membranes containing 3 and 4 wt% PNIPAAm that

presents homogenous dope solution for electrospinning and hence optimal distribution of PNIPAAm on the membrane surface, forming stable hydrogen bonding with water which results in better hydrophilicity compared to other membranes. Figure 3b shows the dynamic CA_w at 50°C of all membranes. For control membrane, the CA_w attenuation was similar at both 22°C and 50°C exhibiting no thermal response. The initial CA_w values for all PNIPAAm containing membranes were higher at 50°C compared to those at 22°C, owing to the contraction state of the polymer chains above LCST resulting in relatively hydrophobic surface property. Generally, at 50°C, the PNIPAAm containing membranes show less significant reduction in CA_w compared to the control membrane. For example, the CA_w of membrane with 4 wt% PNIPAAm at 22°C decreased from 56° to below 11° after 60 s, while it only declined from 77° to 50° when measured at 50°C. The lower reduction of CA_w is ascribed to the hydrophobic coiled shrinkage of PNIPAAm above its LCST that hinders the diffusion of water on the membrane surface.

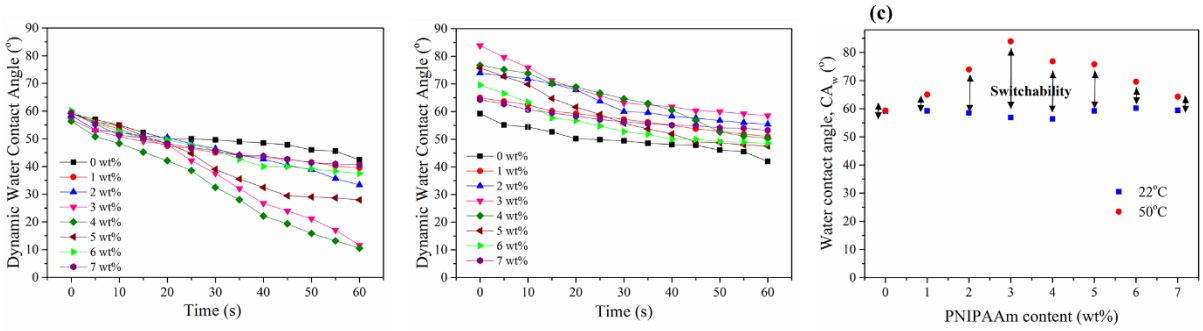

Figure 3. Dynamic water contact angles (CA_w) of the thermo-responsive membranes with contact time for 60 s at (a) 22°C, (b) 50°C; and (c) thermo-switchable CA_w of thermo-responsive membranes at 22°C and 50°C

The thermo-switchable CA_w of the membranes was investigated through measuring their initial CA_w by switching the temperature between 22°C and 50°C. The results are presented in Figure 3c via double arrows indicating the swelling and deswelling states of the polymer chains. It

was observed that the control membrane exhibited no CA_w switchability. In contrast, the membranes containing 1 to 7 wt% PNIPAAm showed switchable CA_w between 22°C and 50°C. Specifically, membranes with 3 and 4 wt% PNIPAAm exhibited the most significant CA_w switchability from 56.9° to 83.9° and from 56.4° to 76.8°, at the respectively, corresponding to the respective swelling and deswelling states induced by the VPT of PNIPAAm, This again could be attributed to the homogeneous distribution of PNIPAAm polymer in the dope solution and hence on the membrane surface via the formation of optimally interconnected nanofibres and nano-nets, which was confirmed by the surface morphology in Figure 1.

3.3. Membrane performance evaluation

Figure 4a shows the clean water permeance for PVDF/nylon-6,6/PNIPAAm membranes and the control at 22°C. It can be noticed that the addition of PNIPAAm into membranes caused a significant decline in water permeance. Specifically, the overall water permeance of control membrane was 849 $L.m^{-2}.h^{-1}.bar^{-1}$, which is much higher than that of the PNIPAAm containing membranes, for example, 46% higher than that for the membrane with 1 wt% PNIPAAm. This permeance decline was attributed to a combination of changes in membrane properties such as nanofibre diameter, membrane thickness, pore size distribution and hydrophilicity that may increase the mass transfer resistance. The overall water permeance of the membrane with 6 and 7 wt% PNIPAAm was the highest (about 640 $L.m^{-2}.h^{-1}.bar^{-1}$), and it decreased with descending PNIPAAm concentration to 552 $L.m^{-2}.h^{-1}.bar^{-1}$ at 1%. Interestingly, the water permeance of the thermo-responsive membrane in this work was at least 3-fold higher than the previously reported PVDF-g-PNIPAAm [40] and PVDF/PNIPAAm (blended) membranes [41] respectively, operated at the same feed pressure of 100 kPa at ambient temperature.

The water permeance and solute rejection of the thermo-responsive membranes were evaluated using the model feed solution in dead end UF mode. The results are shown in Figure 4b. It is observed that the permeance declined consistently with the amount of incorporated PNIPAAm due to the combined changes of membrane properties including morphology (Figure 1), pore structure (Figure 2) and surface wettability (Figure 3). On the other hand, an increasing trend of the BSA rejection rates was observed from 71.4% for the control membrane to 96.6% for the membrane with 4 wt% PNIPAAm.. Although the 4 wt% PNIPAAm membrane exhibited pore size of ~20nm, its high rejection to BSA protein (~7nm [35]) can be explained via the following mechanism: 1) the electrostatic repulsion of negatively charged proteins from the membrane pores as indicated in our previous study on nanofibre-based PVDF membranes [13] and literature [42]; 2) the formation of nanomaterials on the microstructure substrate resulted in multi-scale morphology and was known to induce synergistic effect that enhance the rejection performance [43]; 3) the inter- (protein-protein) and intra-molecular (protein-mineral) interactions commonly result in agglomeration of solutes in the solution and hence improve rejection. However, a further increase in PNIPAAm content from 5 to 7 wt% in membranes cause a decrease in BSA rejection down to 77.2% at 7 wt% owing to uneven pore distribution (Figure 2) and variation in morphological structure (Figure 1). Overall, the responsive membranes with 3 and 4 wt% PNIPAAm present the optimal rejection of protein, which is also consistent with their most sensitive switchability of water contact angle amongst all thermo-responsive membranes (Figure 3). In addition, the BSA rejection of the composite membrane with 4 wt% PNIPAAm was noted to be higher than that of the PVDF/PNIPAAm blend membrane reported in literature as 78% [41], which may be attributed to the formation of the nanonets on the membrane surface (Figure 1) and variation of surface hydrophilicity due to the incorporation of PNIPAAm, as well as the integration between the nanofibre layer and PVDF

substrate that results in the formation of pore structure suitable for UF applications to achieve both high permeability and solute rejection. [13].

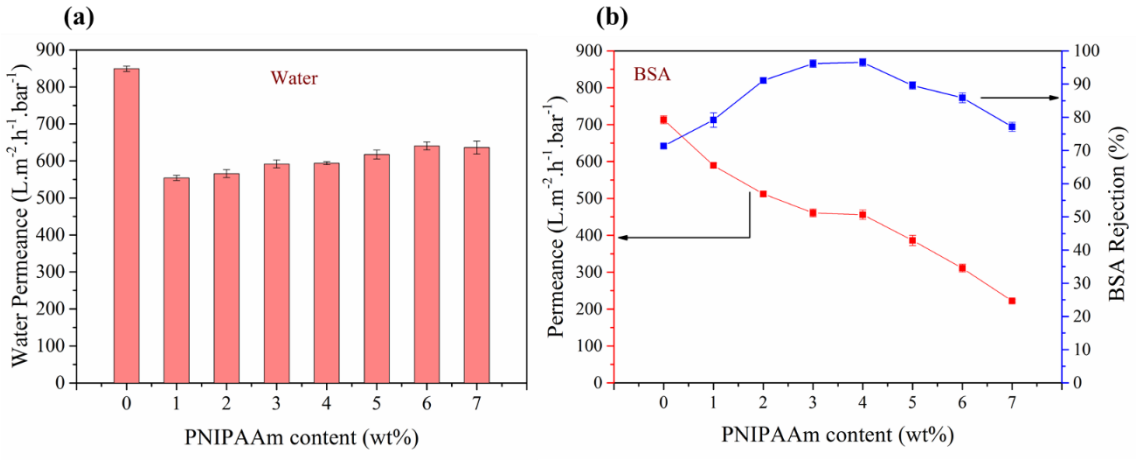

Figure 4. Filtration performance of control and PVDF/nylon-6,6/PNIPAAm membranes containing 1 to 7 wt% PNIPAAm at room temperature and 100 kPa pressure in dead-end stirred cell (a) Clean water permeance with 50 mg/L NaCl solution; (b) Water permeance and BSA rejection with 1,000 mg/L BSA and 50 mg/L NaCl solution.

With the control membrane as benchmark, the thermo-responsive self-cleaning ability of the PNIPAAm membranes was revealed through a series of filtration experiments with BSA solution containing $CaCl_2$. In particular, the composite membranes with no PNIPAAm, 2, 4 and 6 wt% PNIPAAm was investigated through fouling experiments. The results are shown in Figure 5, where (1) Figure 5a shows the water permeance results of all membranes from continuous filtration of BSA solution at 22°C without intermediate cleaning; (2) Figure 5b shows the water permeance throughout the compaction test with DI water at 22°C, followed by two consecutive filtration cycles with the model BSA solution at 22°C with intermediate temperature cleaning at 50°C; (3) Figure 5c compares the results of the 4% PNIPAAm membrane with intermediate cleaning at 22°C and 50°C, respectively. Lastly, Figure 5d summarizes the rate of permeance decline (R_{PD}) that was calculated to indicate the protein

406 fouling resistance of the as-prepared membranes, based on the permeance patterns observed in
407 Figure 5b.

408 Firstly, Figure 5a shows continuous decline in permeance for all membranes indicating that
409 regardless of membrane types, fouling has continued to develop at 22°C and without
410 intermediate cleaning. However, the membrane with 4 wt% PNIPAAm shows the slowest
411 decline, which is consistent with its more hydrophilic property at 22°C (Figure 2). Secondly,
412 the results in Figure 5b show that in the initial compaction tests with DI water, the thermo-
413 responsive membranes exhibited lower initial water permeance compared to the control
414 membrane, which is consistent with the observation in Figure 4. This is attributed to the
415 addition of PNIPAAm instigating changes in pore size distribution caused by an increase in
416 nanofibre diameter and increased membrane thickness (Table S2). The overall pattern of
417 permeance for membranes with PNIPAAm, throughout the filtration study, is flatter than that
418 of the control membrane, indicating better recovery of performance after temperature cleaning.
419 In particular, the membrane with 4 wt% PNIPAAm was found most promising with minimal
420 permeance decline compared to other membranes, i.e., in the second filtration cycle with the
421 BSA solution, the temperature cleaning at 50°C for membrane with 4 wt% PNIPAAm was
422 most effective to recover 96% of the first cycle permeance; whereas the membranes with 2 and
423 6 wt% PNIPAAm recovered about 67% and 75% of the first cycle permeance, respectively,
424 as compared to the control membrane with only 56% permeance recovery. The higher
425 permeance recovery by membrane containing 4 wt% PNIPAAm as a result of self-cleaning is
426 ascribed to the good surface hydrophilicity (Figure 2a) and inherent washing force provided by
427 the conformational volume-phase transition causing the PNIPAAm polymer chain to stretch
428 and shrink [30]. The optimal results achieved with the 4 wt% PNIPAAm compared to 2 and 6
429 wt% PNIPAAm are attributed to stronger thermo-switchability as indicated via the CA_w of the
430 respective membranes (Figure 3). Previous studies also found that the protein

adsorption/desorption behaviour of PNIPAAm modified surfaces could be related to combined effects of physical properties, i.e., surface wettability, PNIPAAm content/density and polymer molecular weight, which could play a key role in forming anti-fouling surfaces as filtration membranes [23].

Further confirmation of the role of thermo-responsivity on fouling control, the 4% PNIPAAm membrane was selected to compare the performance with intermediate cleaning at 22°C and 50°C, respectively. It was shown that for the 4 wt% PNIPAAm membrane the intermediate temperature cleaning at 50°C was more effective than that at 22°C, confirming the incorporation of PNIPAAm has reduced the attachment of protein foulants, due to the conformational volume-phase transition as the solution temperature was switched from below (i.e., 22°C) to above (i.e., 50°C) the LCST during intermediate cleaning. Also, it is noted that the pure water permeance during cleaning at 50°C increased, as shown in Figure 5b and 5c, which can be explained by the shrunken state of the PNIPAAm chains that resulted in enlarged pore size [34], again demonstrating the thermo-responsive property of the membrane.

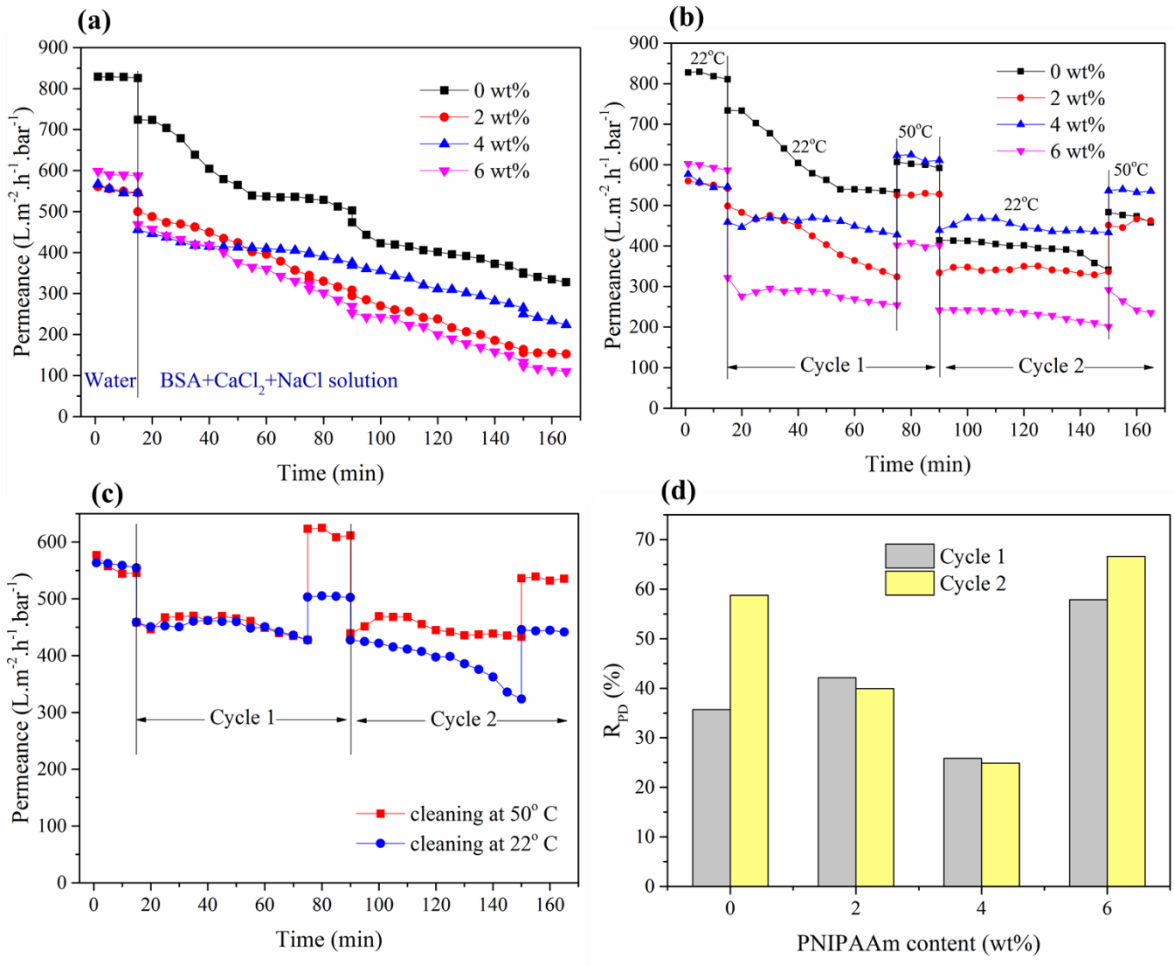

446

447 **Figure 5.** Protein fouling studies for control and PVDF/nylon-6,6/PNIPAAm membranes
448 containing 2, 4 and 6 wt% PNIPAAm. (a) Permeance of continuous filtration test without
449 intermediate cleaning. (b) Permeance of filtration test with intermediate temperature cleaning
450 at 50°C.(c) Comparison of permeance of filtration test with intermediate cleaning at 22°C and
451 50°C for membrane containing 4 wt% PNIPAAm. (d) R_{PD} for 2 filtration cycles with 50°C
452 cleaning illustrated in Fig 6b. Experimental Conditions: Pressure = 100 kPa, cross-flow
453 velocity = 12.6 $cm.s^{-1}$, feed solution containing 1 g/L BSA, 1 mM $CaCl_2$ and 7 mM NaCl.

454

455 Based on the permeance patterns observed for all membranes in Figure 5b, the rate of
456 permeance decline (R_{PD}) was calculated and summarized in Figure 5d to indicate the protein
457 fouling resistance. During the first filtration cycle, the thermo-responsive membrane containing
458 4 wt% PNIPAAm exhibited the lowest R_{PD} of 26%, compared to others membranes including
459 the control with an R_{PD} of 36%. Relatively membranes with 2 and 6 wt% PNIPAAm also had

higher R_{PD} of 42% and 58% respectively. The lower R_{PD} of membrane containing 4 wt% PNIPAAm was attributed to the decreased surface-protein interaction resisting BSA adsorption as a result of improved hydrophilicity (Figure 2a), higher steric repulsion and water hydration forces by the addition of PNIPAAm [32]. The results were promising when compared to the literature reported PVDF-g-PNIPAAm membrane having a permeance recovery of 80% in 30 min of filtration using a pure BSA solution of 0.5 g/L [40]; while the current as-prepared membrane containing 4 wt% PNIPAAm showed a permeance recovery of 91% in 30 min filtration (Figure 5d) using a more realistic model feed solution containing BSA, $CaCl_2$ and NaCl, which simulates a more complex yet practical fouling environment. This confirmed the theory that the improved hydrophilicity below LCST and more significant thermal switchability leading to stronger segment mobility of polymer chains are beneficial for reducing protein adsorption [26].

Further, during the second filtration cycle, the membranes exhibited distinct fouling behaviours with an increased R_{PD} of 59%, 40% and 67% for membrane containing no (control), 2 and 6 wt% PNIPAAm, respectively; whereas the R_{PD} for membrane with 4 wt% PNIPAAm remained almost the same (25%). The trends of permeance decline and post-cleaning recovery can be further confirmed by the morphological changes in the filtrati. /on study, as shown in SEM images of fouled membranes in Figure 6. The membranes containing 2 and 4 wt% PNIPAAm showed much reduced protein deposition presenting clear surface compared to the membranes containing no PNIPAAm and 6 wt% PNIPAAm that showed heavy fouling. This is attributed to the lower R_{PD} of membrane containing 4 wt% PNIPAAm and better thermo-switchable contact angles causing similar volume phase transition during cleaning compared to other membranes.

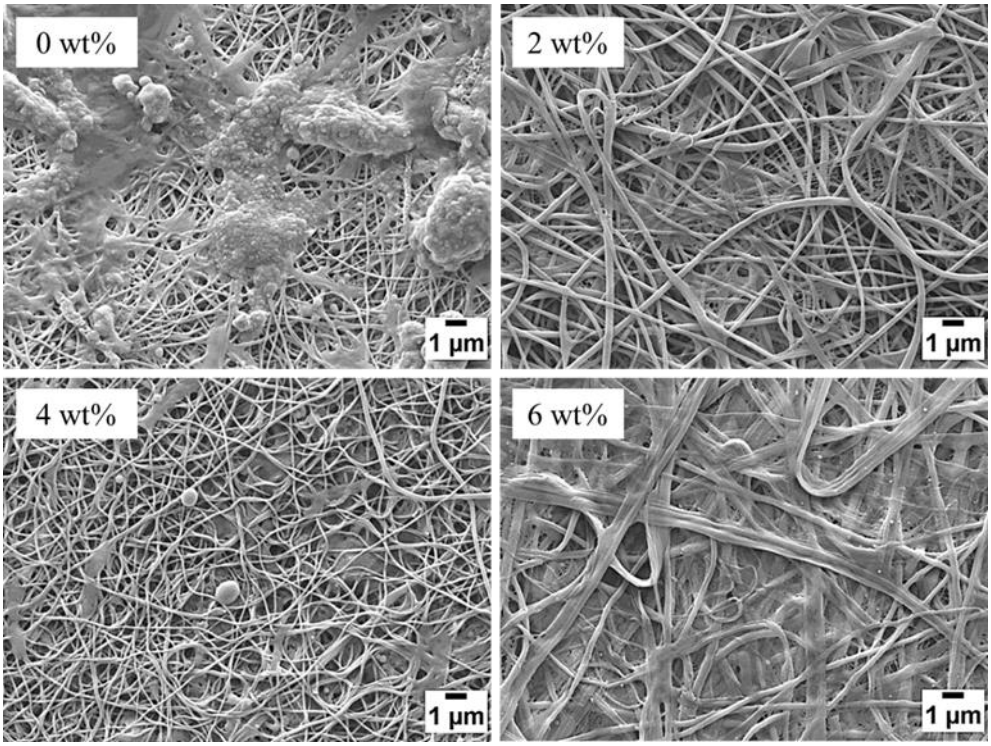

Figure 6. SEM images of protein fouled control and PVDF/nylon-6,6/PNIPAAm membranes containing 2, 4 and 6 wt% PNIPAAm after two filtration cycles (Experimental conditions: pressure = 100 kPa, cross-flow velocity = 12.6 $cm.s^{-1}$, feed solution = 1 g/L BSA, 1 mM $CaCl_2$ and 7 mM NaCl)

Overall, the membrane containing 4 wt% PNIPAAm revealed superior fouling resistance with reduced protein-surface interactions, led to lower permeance decline after each BSA filtration cycle and more effective intermediate cleaning. The much higher permeance recovery in each cycle after the temperature-change intermediate cleaning was contributed by the self-cleaning property of membrane based on the following theories: 1) the improved surface hydrophilicity allows less interaction of proteins with the membrane; 2) the temperature-change cleaning between the filtration cycles provides the washing force for disrupting the protein fouling layer due to the alternating polymer chain contraction (>LCST) and stretching (<LCST) induced by volume-phase transition, which causes the formation of inter- and intra-molecular hydrogen bonds between the hydrophilic moieties of PNIPAAm and the water molecules [31]. Overall,

500 the surface wettability and nano-topography of the proposed composite membranes were
501 considered responsible for enhancing the thermo-responsivity and hence improving anti-
502 fouling and self-cleaning effects during filtration.

503 **4. Conclusions**

504 In this work a highly protein-fouling-resistant and self-cleaning PVDF/nylon-
505 6,6/PNIPAAm composite ultrafiltration membrane was fabricated via a two-step
506 electrospinning and conventional casting process. The morphological analysis of PVDF/nylon-
507 6,6/PNIPAAm membranes demonstrated non-homogenous distribution of nano-net structures
508 on the membrane surface that affected the pore size distribution and solute rejection of the
509 membranes. Compared to control membrane, the PVDF/nylon-6,6/PNIPAAm membrane
510 exhibited good antifouling properties and improved membrane performance during filtration
511 of feed solution containing BSA, $CaCl_2$ and NaCl. Following a facile intermediate temperature
512 change cleaning from 22°C to 50°C, the thermo-responsive membrane showed the best
513 recovery of water permeance, where the detachment of absorbed proteins could be explained
514 by the improved surface hydrophilicity below LCST and segment mobility of polymer chain
515 induced by volume-phase transitional of PNIPAAm at switchable temperatures. Therefore, the
516 as-developed PVDF/nylon-6,6/PNIPAAm composite membrane with self-cleaning surface has
517 great potential in treating effluents with protein foulants. Future studies could be done to
518 explore the ability of the proposed membrane in the applications involving complex real
519 wastewater matrices such as the combined effect of polysaccharides (e.g., humic acid) and
520 macromolecules (e.g., proteins). Systematic investigations on the inter- and intra-foulant-
521 species interactions, and foulant-membrane interactions associated with the thermo-responsive
522 effect of the membrane material would be of great interest and beneficial for industrial
523 applications in the field of wastewater treatment, food and bioprocessing.

Acknowledgements

This work was supported by Victoria India Institute via Victoria India Doctoral Scholarship. Dr. L. DUMEE acknowledges the Australian Research Council (ARC) for his DECRA fellowship (DE180100130). Dr Xing Yang would like to acknowledge Victoria University for the Industry Postdoctoral Fellowship. The Microscopy platform at Deakin University and support from the technical team is also acknowledged.

Notes

The authors declare no competing financial interest.

Supporting Information:

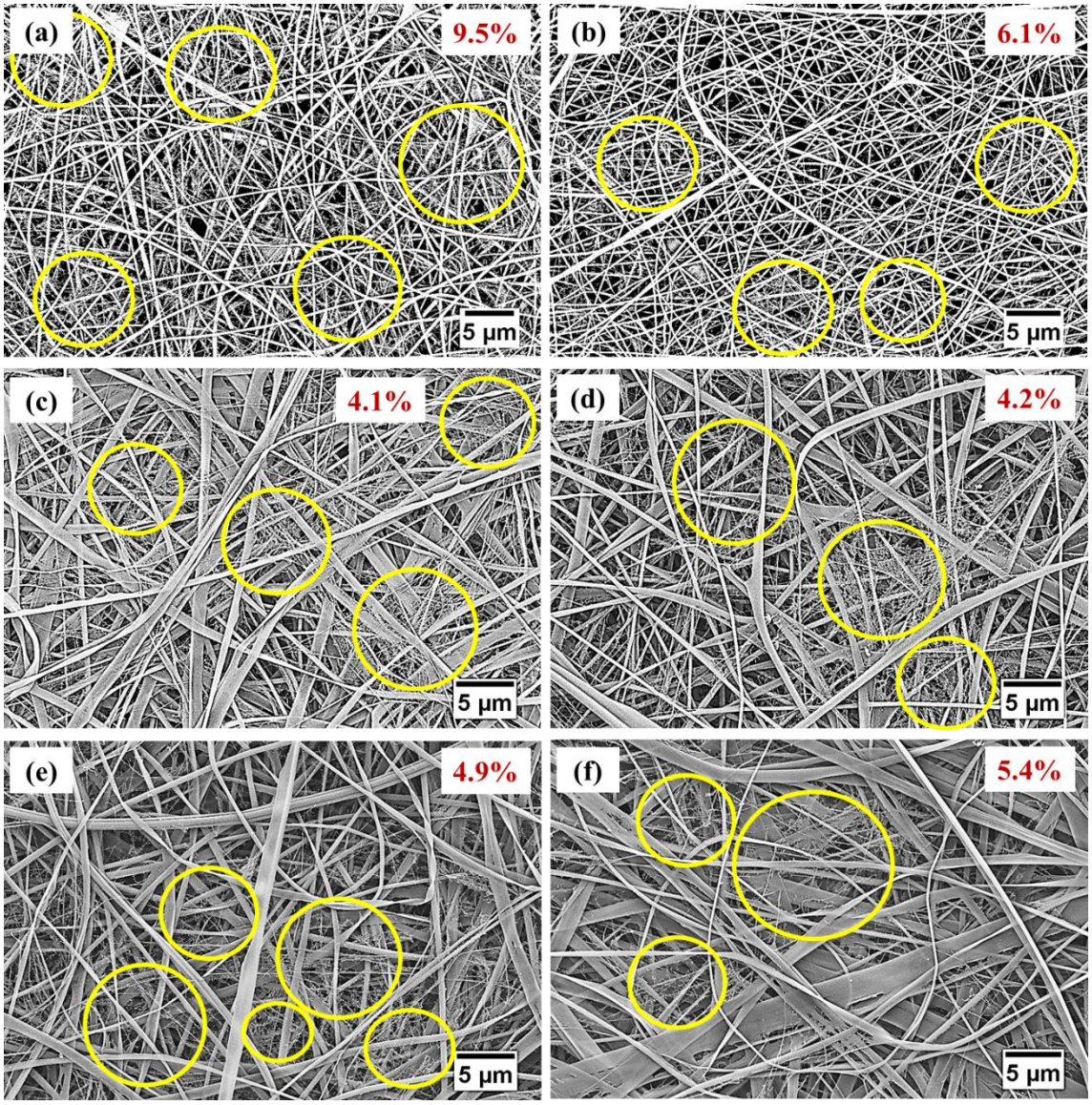

Figure S1. SEM images of PVDF/nylon-6,6/PNIPAAm membrane surfaces with (a) 2 wt%, (b) 3 wt%, (c) 4 wt%, (d) 5 wt%, (e) 6 wt% and (f) 7 wt% PNIPAAm and the percentage density of nanonets including the selected areas (in yellow).

562 **Table S1.** Physical properties of PVDF/nylon-6,6/PNIPAAm membranes

PNIPAAm content (wt%)	Main nanofiber diameter (nm)	Membrane thickness (μm)	Mean pore size (nm)	Modulus of elasticity (MPa)
0	83±27	245±8	47	35.12
1	93±18	247±7	48	45.36
2	177±18	254±8	36	24.59
3	229±18	259±9	32	31.08
4	312±63	263±12	26	30.11
5	479±130	266±10	48	24.91
6	812±409	270±10	52	46.06
7	500±216	272±12	58	48.42

563

564

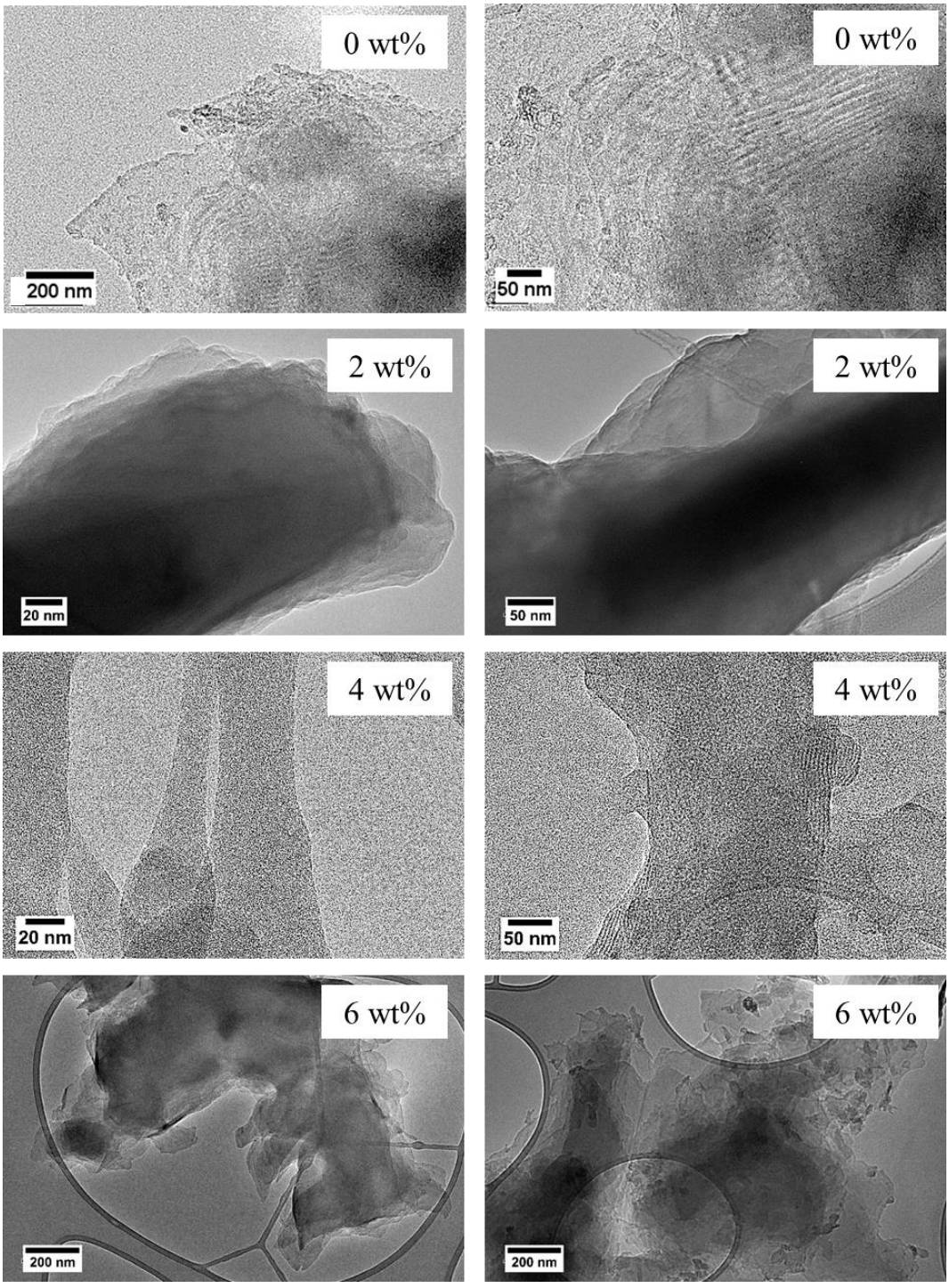

Figure S2. TEM images of PVDF/nylon-6,6/PNIPAAm fibres with 0, 2, 4 and 6 wt% PNIPAAm. The large thickness of the fibres prevented appropriate imaging of their structure. The TEM sample preparation was difficult due to the strong agglomeration of the fibres. The sonication in water supported the formation of smaller fibre clusters.

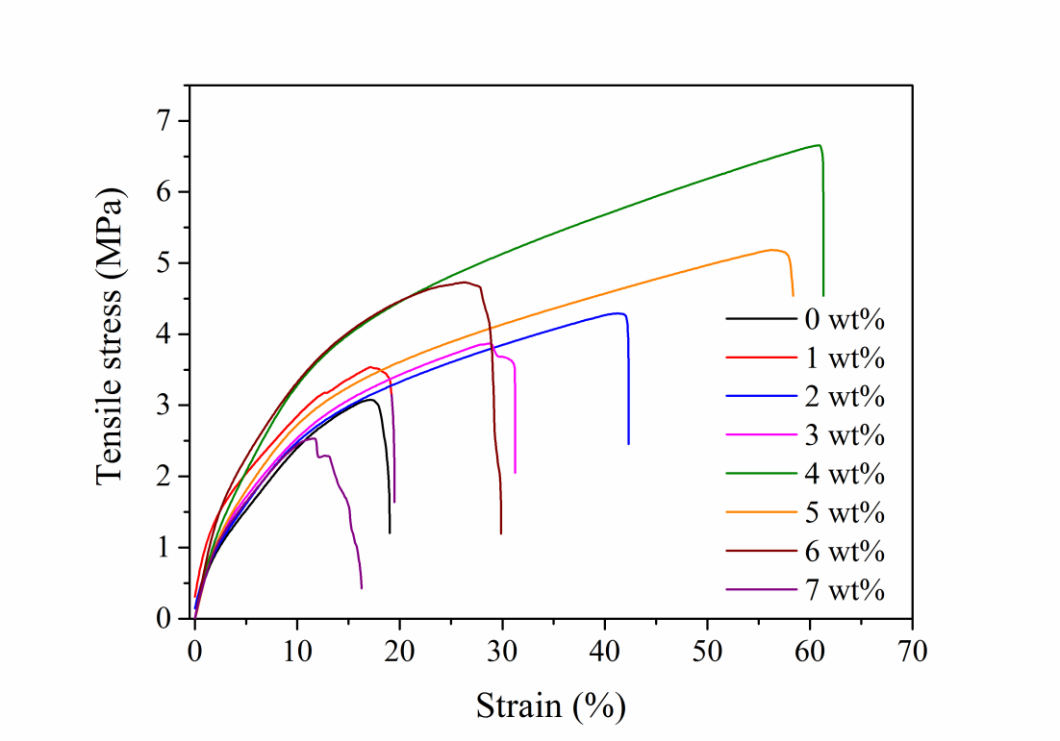

570

571 **Figure S3.** Stress vs strain curves of control and PVDF/nylon-6,6/PNIPAAm membranes with
572 1 wt% to 7 wt% PNIPAAm.

573

574

575

576

577

References

[1] H. Susanto and M. Ulbricht, Influence of ultrafiltration membrane characteristics on adsorptive fouling with dextrans, Journal of Membrane Science, 266 (1) (2005) 132-142

[2] K. J. Jim, A. G. Fane, C. J. D. Fell and D. C. Joy]Fouling mechanisms of membranes during protein ultrafiltration, Journal of Membrane Science, 68 (1) (1992) 79-91

[3] C.-C. Ho and A. L. Zydney, A Combined Pore Blockage and Cake Filtration Model for Protein Fouling during Microfiltration, Journal of Colloid and Interface Science, 232 (2) (2000) 389-399

[4] X. Shi, G. Tal, N. P. Hankins and V. Gitis, Fouling and cleaning of ultrafiltration membranes: A review, Journal of Water Process Engineering, 1 (2014) 121-138

[5] Ś. F. E. Boerlage, M. D. Kennedy, M. p. Aniye, E. M. Abogrean, D. E. Y. El-Hodali, Z. S. Tarawneh and J. C. Schippers, Modified Fouling Indexultrafiltration to compare pretreatment processes of reverse osmosis feedwater, Desalination, 131 (1) (2000) 201-214

[6] Z. Zhao, J. Zheng, M. Wang, H. Zhang and C. C. Han, High performance ultrafiltration membrane based on modified chitosan coating and electrospun nanofibrous PVDF scaffolds, Journal of Membrane Science, 394–395 (2012) 209-217

[7] Q. Shi, Y. Su, X. Ning, W. Chen, J. Peng and Z. Jiang, Trypsin-enabled construction of anti-fouling and self-cleaning polyethersulfone membrane, Bioresource Technology, 102 (2) (2011) 647-651

[8] L.-P. Zhu, Z. Yi, F. Liu, X.-Z. Wei, B.-K. Zhu and Y.-Y. Xu, Amphiphilic graft copolymers based on ultrahigh molecular weight poly(styrene-alt-maleic anhydride) with poly(ethylene glycol) side chains for surface modification of polyethersulfone membranes, European Polymer Journal, 44 (6) (2008) 1907-1914

[9] S. Chede and I. C. Escobar, Fouling control using temperature responsive N-isopropylacrylamide (NIPAAm) membranes, Environmental Progress & Sustainable Energy, 35 (2) (2016) 416-427

[10] X. Zhao and C. He, Efficient Preparation of Super Antifouling PVDF Ultrafiltration Membrane with One Step Fabricated Zwitterionic Surface, ACS Applied Materials & Interfaces, 7 (32) (2015) 17947-17953

[11] J. A. Prince, S. Bhuvana, V. Anbharasi, N. Ayyanar, K. V. K. Boodhoo and G. Singh, Self-cleaning Metal Organic Framework (MOF) based ultra filtration membranes - A solution to bio-fouling in membrane separation processes, Sci. Rep., 4 (2014)

[12] D. Rana and T. Matsuura, Surface Modifications for Antifouling Membranes, Chemical Reviews, 110 (4) (2010) 2448-2471

[13] A. Vanangamudi, L. F. Dumée, M. C. Duke and X. Yang, Nanofiber Composite Membrane with Intrinsic Janus Surface for Reversed-Protein-Fouling Ultrafiltration, ACS Applied Materials & Interfaces, 9 (21) (2017) 18328-18337

[14] J. Miller Daniel, R. Dreyer Daniel, W. Bielawski Christopher, R. Paul Donald and D. Freeman Benny, Surface Modification of Water Purification Membranes, Angewandte Chemie International Edition, 56 (17) (2016) 4662-4711

[15] N. Shahkaramipour, T. Tran, S. N. Ramanan and H. Lin, 7, Membranes with Surface-Enhanced Antifouling Properties for Water Purification, 2017

[16] S. K. Vakkalanka, C. S. Brazel and N. A. Peppas, Temperature- and pH-sensitive terpolymers for modulated delivery of streptokinase, Journal of Biomaterials Science, Polymer Edition, 8 (2) (1997) 119-129

[17] L. Ying, E. T. Kang, K. G. Neoh, K. Kato and H. Iwata, 243, Drug permeation through temperature-sensitive membranes prepared from poly(vinylidene fluoride) with grafted poly(N-isopropylacrylamide) chains, 2004

[18] S. Lanzalaco and E. Armelin, Poly(N-isopropylacrylamide) and Copolymers: A Review on Recent Progresses in Biomedical Applications, Gels, 3 (4) (2017)

[19] H. Bae You, T. Okano and W. Kim Sung, Temperature dependence of swelling of crosslinked poly(N,N′-alkyl substituted acrylamides) in water, Journal of Polymer Science Part B: Polymer Physics, 28 (6) (2003) 923-936
[20] Y. Xu, L. Shi, R. Ma, W. Zhang, Y. An and X. X. Zhu, Synthesis and micellization of thermo- and pH-responsive block copolymer of poly(N-isopropylacrylamide)-block-poly(4-vinylpyridine), Polymer, 48 (6) (2007) 1711-1717
[21] M. Heskins and J. E. Guillet, Solution Properties of Poly(N-isopropylacrylamide), Journal of Macromolecular Science: Part A - Chemistry, 2 (8) (1968) 1441-1455
[22] A. K. Lele, I. Devotta and R. A. Mashelkar, Predictions of thermoreversible volume phase transitions in copolymer gels by lattice-fluid-hydrogen-bond theory, The Journal of Chemical Physics, 106 (11) (1997) 4768-4772
[23] C. C. Michael, G. T. Ryan and D. G. Nathan, Protein-surface interactions on stimuli-responsive polymeric biomaterials, Biomedical Materials, 11 (2) (2016) 022002
[24] J. Kobayashi, Y. Arisaka, N. Yui, Y. Akiyama, M. Yamato and T. Okano, Effect of Temperature Changes on Serum Protein Adsorption on Thermoresponsive Cell-Culture Surfaces Monitored by A Quartz Crystal Microbalance with Dissipation, International Journal of Molecular Sciences, 19 (5) (2018) 1516
[25] J. H. Lee, H. B. Lee and J. D. Andrade, Blood compatibility of polyethylene oxide surfaces, Progress in Polymer Science, 20 (6) (1995) 1043-1079
[26] D. Gan and L. A. Lyon, Synthesis and Protein Adsorption Resistance of PEG-Modified Poly(N-isopropylacrylamide) Core/Shell Microgels, Macromolecules, 35 (26) (2002) 9634-9639
[27] I. Kiesel, M. Paulus, J. Nase, S. Tiemeyer, C. Sternemann, K. Rüster, F. J. Wirkert, K. Mende, T. Büning and M. Tolan, Temperature-Driven Adsorption and Desorption of Proteins at Solid–Liquid Interfaces, Langmuir, 30 (8) (2014) 2077-2083
[28] H. Shen, L. J. Tauzin, W. Wang, B. Hoener, B. Shuang, L. Kisley, A. Hoggard and C. F. Landes, Single-Molecule Kinetics of Protein Adsorption on Thin Nylon-6,6 Films, Analytical Chemistry, 88 (20) (2016) 9926-9933
[29] R. Ou, J. Wei, L. Jiang, G. P. Simon and H. Wang, Robust Thermoresponsive Polymer Composite Membrane with Switchable Superhydrophilicity and Superhydrophobicity for Efficient Oil–Water Separation, Environmental Science & Technology, 50 (2) (2016) 906-914
[30] Y. Ye, J. Huang and X. Wang, Fabrication of a Self-Cleaning Surface via the Thermosensitive Copolymer Brush of P(NIPAAm-PEGMA), ACS Applied Materials & Interfaces, 7 (40) (2015) 22128-22136
[31] S. Zhou, A. Xue, Y. Zhang, M. Li, J. Wang, Y. Zhao and W. Xing, Fabrication of temperature-responsive ZrO2 tubular membranes, grafted with poly (N-isopropylacrylamide) brush chains, for protein removal and easy cleaning, Journal of Membrane Science, 450 (2014) 351-361
[32] B. P. Tripathi, N. Dubey, F. Simon and M. Stamm, 4, Thermo responsive ultrafiltration membranes of grafted poly(N-isopropyl acrylamide) via polydopamine, 2014
[33] Q. Zhou, J.-h. Li 李建华, B.-f. Yan, D. Wu 吴东 and Q.-q. Zhang 张其清, 32, Thermo-responsive and antifouling PVDF nanocomposited membranes based on PNIPAAm modified TiO2 nanoparticles, 2014
[34] H. Guo, J. Huang and X. Wang, The alternate temperature-change cleaning behaviors of PNIPAAm grafted porous polyethylene membrane fouled by proteins, Desalination, 234 (1) (2008) 42-50
[35] R. Miao, L. Wang, L. Feng, Z.-W. Liu and Y.-T. Lv, Understanding PVDF ultrafiltration membrane fouling behaviour through model solutions and secondary wastewater effluent, Desalination and Water Treatment, 52 (25-27) (2014) 5061-5067
[36] M. Khaldi, P. Blanpain-Avet, R. Guérin, G. Ronse, L. Bouvier, C. André, S. Bornaz, T. Croguennec, R. Jeantet and G. Delaplace, Effect of calcium content and flow regime on whey protein fouling and cleaning in a plate heat exchanger, Journal of Food Engineering, 147 (2015) 68-78

[37] H. Pant, B. Pant, P. Pokharel, H. Joo Kim, L. Tijing, C. Park, D.-S. Lee, H. Kim and C. Sang Kim, 429, Photocatalytic TiO2–RGO/nylon-6 spider-wave-like nano-nets via electrospinning and hydrothermal treatment, 2013

[38] Z. Li, Y. Xu, L. Fan, W. Kang and B. Cheng, Fabrication of polyvinylidene fluoride tree-like nanofiber via one-step electrospinning, Materials & Design, 92 (2016) 95-101

[39] B. Cheng, Z. Li, Q. Li, J. Ju, W. Kang and M. Naebe, Development of smart poly(vinylidene fluoride)-graft-poly(acrylic acid) tree-like nanofiber membrane for pH-responsive oil/water separation, Journal of Membrane Science, 534 (2017) 1-8

[40] Y. Zhao, H. Zhao, L. Chen, X. Feng, Q. Zhang, J. Wang and R. Zhang, Thermo-responsive modification and properties study of PVDF flat membrane, Journal of Polymer Research, 20 (1) (2012) 58

[41] X. Chen, C. Shi, Z. Wang, Y. He, S. Bi, X. Feng and L. Chen, Structure and performance of poly(vinylidene fluoride) membrane with temperature - sensitive poly(n - isopropylacrylamide) homopolymers in membrane pores, Polymer Composites, 34 (4) (2013) 457-467

[42] A. I. C. Morão, A. M. B. Alves and M. D. Afonso, Concentration of clavulanic acid broths: Influence of the membrane surface charge density on NF operation, Journal of Membrane Science, 281 (1) (2006) 417-428

[43] J. Zhang, Z. Xu, W. Mai, C. Min, B. Zhou, M. Shan, Y. Li, C. Yang, Z. Wang and X. Qian, Improved hydrophilicity, permeability, antifouling and mechanical performance of PVDF composite ultrafiltration membranes tailored by oxidized low-dimensional carbon nanomaterials, Journal of Materials Chemistry A, 1 (9) (2013) 3101-3111